Research Article

Pluronic-Coated Biogenic Gold Nanoparticles for Colon Delivery of 5-Fluorouracil: *In vitro* and *Ex vivo* Studies

Wael A. Mahdi,[1,6] Afzal Hussain,[1,6] Mohd Ramzan,[2,3] Abdul Faruk,[4] Sarah I Bukhari,[1] and Abhimanyu Dev[5]

Abstract. The aim of the study was to prepare 5-fluorouracil (5-FU)-loaded biogenic gold nanoparticles with pluronic-based coating (PFGNPs), their optimization (full factorial predicted OBPN-1) and *in vitro-ex vivo* evaluation. Several formulations were prepared, selected for optimization using Design Expert®, and compared for morphology, 5-FU release kinetics, compatibility, cell line toxicity, *in vitro* hemocompatibility, and *ex vivo* intestinal permeation across the rat duodenum, jejunum, and ileum. The pluronic-coated 5-FU-carrying GNPs were spherical, 29.11–178.21 nm in diameter, with a polydispersity index (PDI) range of 0.191–292, and a zeta potential (ZP) range of 11.19–29.21 (-mV). The optimized OBPN-1 (desirability = 0.95) demonstrated optimum size (175.1 nm), %DL as 73.8%, ZP as 21.7 mV, % drug release (DR) as 75.7%, and greater cytotoxicity (viability ~ 8.9%) against the colon cancer cell lines than 5-FU solution (~ 24.91%), and less hemocompatibility. Moreover, OBPN-1 exhibited 4.5-fold permeation across the rat jejunum compared with 5-FU solution. Thus, the PFGNPs exhibit high DL capacity, sustained delivery, hemocompatibility, improved efficacy, and enhanced permeation profiles compared with 5-FU solution and several other NPs preparations suggesting it is a promising formulation for effective colon cancer control with reduced side effects.

KEY WORDS: biogenic gold nanoparticles; Design Expert®; colon cancer cell lines; hemolysis assessment; *ex vivo* permeation profiles.

INTRODUCTION

Cancer was the second leading cause of premature death globally in 2018 according to the World Health Organization. Of the 9.6 million deaths in 2018, an estimated 1.8 million was due to colon cancer and other cancers such as those of the lungs and breast (4.18 million), prostate (~ 1.28 million), skin (~ 1.04 million), and stomach (~ 1.03 million) (1). Smoking, air pollution, and genetic susceptibility are the primary risk factors for lung cancer and the associated mortality (2). The thymidylate synthase inhibitor 5-fluorouracil (5-FU) suppresses tumor growth by integration into cellular DNA (deoxyribonucleic acid) and RNA (ribonucleic acid), resulting in cell cycle arrest at the S phase (3–5). While 5-FU is considered a first-line treatment for solid tumors, its clinical application is limited by gastrointestinal disturbances, bone marrow toxicity, systemic toxicity arising from non-specificity of tumor over normal cells, and by its short plasma half-life necessitating high and frequent dosing (6). Several reports have documented an increased efficacy and reduced toxicity when formulated as nanoparticles (NPs) with surface functionalization (7, 8). For instance, a 5-FU-loaded chitosan/gold nanocomposite demonstrated an epitome proficiency of 96% (9). High drug loading (DL) efficiency (%DL), targeted drug delivery, enhanced drug access to the site of action, and carrier biocompatibility are considered the most important attributes of such drug delivery systems for cancer treatment (10).

Poly lactic-co-glycolic acid (PLGA) and pluronic F-127 are biocompatible and biodegradable copolymers responsible for high %DL, efficiency, and controlled release kinetics (11, 12). Pluronic has several advantages over PLGA, which have attracted attention in the field of chemotherapy and formulation development, including (a) their nontoxic and non-ionic nature, (b) excellent selectivity against multidrug-resistant cells by inhibiting p-glycoprotein efflux, (c)

---

[1] Department of Pharmaceutics, College of Pharmacy, King Saud University, Riyadh, 11451, Saudi Arabia.

[2] Department of Pharmaceutics, PCTE Institute of Pharmacy, PTU, Ludhiana, Punjab, India.

[3] Department of Pharmaceutics, University Institute of Pharmaceutical Sciences, Panjab University, Chandigarh, Punjab, India.

[4] Department of Pharmaceutical Science, HNB Garhwal University (A Central University), Srinagar, Uttarakhand, India.

[5] Department of Pharmaceutical Sciences and Technology, Birla Institute of Technology, Mesra, Jharkhand 835215, Ranchi, India.

[6] To whom correspondence should be addressed. (e–mail: wmahdi@ksu.edu.sa; afzal.pharma@gmail.com)

prolonging of systemic circulation time, and (d) enhancing pro-apoptotic signaling thereby sensitizing cancerous cells (13–15). Furthermore, a pluronic- or PLGA-based coating have been reported to prolong drug release, stability, and colon targeting of 5-FU (12, 16, 17). Such PLGA and pluronic-based nanocarriers have demonstrated controlled and efficient delivery of taxol and 5-FU to tumors, respectively (12, 18, 19). Moreover, these nanocarriers have been used to deliver proteins like recombinant human growth hormone, interferon α-2b, bovine serum albumin, vaccines, and antibiotics like 4-hexylresorcinol, rifampicin, and oxolinic acid to specific targets (19–23). Gold NPs are also promising nanocarriers for 5-FU delivery due to several unique advantageous properties, such as their spherical shape, controlled size, high chemical reducing ability, non-toxicity, a tunable surface for functionalization, and optical properties (24). The efficacy of 5-FU for the treatment of colorectal cancer can be improved 2-fold by adding a pluronic F127-based surface coating of gold NPs (12). Furthermore, efficacy can also improve (6.8- and 18.4-fold reduction in tumor volume) by increasing 5-FU permeation to treat a mouse skin cancer model *via* gold NPs coated with cetyl trimethyl ammonium bromide (CTAB) (25, 26). Recently, a biomediated drug-loaded NP (orange juice-based) formulation further increased 5-FU efficacy against murine fibrosarcoma in BALB/c mice suggesting that a biomediated synthesis strategy may be advantageous for drug incorporation and coating (27). Herein, we combined biogenic synthesis of gold NPs using *Bacillus licheniformis (B. licheniformis)* as the reducing agent and a pluronic coating for controlled release and improved efficacy against colon cancer.

These pluronic-coated 5-FU carrying gold NPs (PFGNPs and OBPN-1) were compared with placebo gold NPs (GNPs), PLGA NPs (PNPs), 5-FU carrying NPs (PFNPs), pluronic-coated gold NPs (PGNPs), and 5-FU-loaded gold NPs (FGNPs) for size, zeta potential (ZP), chemical interaction using Fourier transform infrared (FTIR), morphology, *in vitro* release kinetics, DL capacity, *in vitro* hemolysis, and cell cytotoxicity. The three GNP nanoconjugates were also assessed for *ex vivo* permeation profiles across the rat duodenum, jejunum, and ileum.

MATERIALS AND METHODS

Materials

A gram-positive and thermophilic *Bacillus licheniformis* (MTCC 429) was obtained from Indian Institute of Microbial Technology, Chandigarh, Punjab, India. 5-Fluorouracil (5-FU) was gifted from Spectrochem Pvt. Ltd. (Mumbai, India). Chloroauric acid (HAuCl$_4$) as a starting material, pluronic F127 and poly(lacto-co-glycolic) acid (PLGA 50:50) (low molecular weight, 5 kDa) were obtained from Sigma-Aldrich, Mumbai, India, and Purac, Biomaterial (Netherlands), respectively. The human colon cancer cell lines (HCT-116) were obtained from the National Centre for Cell Science (NCCS, India). Dulbecco's modified Eagle's medium (DMEM) supplemented with 10% fetal bovine serum (FBS) was purchased from HiMedia. The culture media was also supplemented with an aqueous solution of 1% penicillin-streptomycin. All other solvents and reagents used were of AR grade. Distilled water was used as aqueous media for buffers and related preparations.

Methods

B. licheniformis Culture and Isolation of Enzyme

The bacteria were revived and sub-cultured as per the manufacturer's protocol (28). The culture was grown in a modified nitrate broth by incubating at 37°C for 24 h under constant shaking (100 rpm) (28, 29). The growth media was supplemented with glucose as a source of carbon. Then, the grown culture (10 mL) was centrifuged at 5000 rpm for 30 min to obtain a pellet, which was further re-suspended in 50 mL of 0.05 M phosphate buffer solution (PBS) and subjected to probe sonication for 5 min with a 30 s on-off cycle (Sonic Vibra Cell VC 130, Newton, USA) to lyse the bacterial cells. The solution was again centrifuged to separate the supernatant containing the enzymes which served as the cellular lysate supernatant (CLS) for the synthesis of the 5-FU-loaded gold NPs (FGNPs). The extracted intracellular enzyme was utilized for the biosynthesis of gold NPs.

In Situ Biogenic Gold, Pluronic-Capped Gold, and Polymeric Nanoparticles

The 5-FU-loaded gold NPs were synthesized as reported with slight modification (28, 30). The extracted CLS (50%, 25 mL) was transferred to a 100-mL Erlenmeyer flask and mixed with chloroauric acid (HAuCl$_4$) (10 mL, 500 mg/L) under constant stirring (150 rpm) followed by incubation at 30°C for 72 h. The final pH was adjusted to 6.0 using 0.1 M sodium hydroxide and 0.1 N HCl. A visible purple color change occurred due to CLS-mediated reduction of Au^{+3} ions in the reaction mixture after 6 h. The reaction mixture was then allowed to stand for an additional 8 h to ensure complete reduction of Au^{+3}. The obtained ruby red-colored colloidal nanosuspension was ultracentrifuged (18,000 rpm, 15 min) to isolate GNPs followed by washing in 10 mM PBS (pH 7.4). The FGNPs were then prepared by incubating GNPs with aqueous 5-FU solution (pH 6.0) under the same experimental conditions. GNPs and the drug-loaded GNPs formulations (10 mL) were coated separately by mixing with an aqueous solution of pluronic polymer (4 mL, 1×10^{-3} M) (12).

To prepare polymeric PNPs, PLGA (150 mg) was dissolved in dichloromethane (DCM) (15 mL) and an aqueous solution of 5-FU (100 mg/10 mL) was carefully added to the organic phase under constant stirring (4000 rpm). The mixture was sonicated for 5 min in 30 pulses (on/off) to obtain a water in oil emulsion. Then, it was injected into a 30 mL aqueous solution containing polyvinyl alcohol (PVA) (1%) as stabilizer under constant stirring followed by sonication for 10 min to obtain PLGA-based NPs. The DCM was evaporated using a rotary evaporator (31).

Physicochemical characterization of nanoparticles

Particle size and size distribution. Mean NP size and size distribution (polydispersity index, PDI) were measured using dynamic light scattering (DLS) (Malvern Inst., UK; Nano ZS

Zetasizer) at a scattering angle of 90°. Samples were first diluted with 100 volumes of distilled water and then sonicated for 2 min in 30-s pulses to guarantee adequate dispersal (32).

Zeta potential (surface charge density). The overall particle surface charge determines the stability of the formulation due to electrostatic repulsion generated amongst the particles. The ZP, which predicts the physical stability of colloidal systems, was measured using a Malvern Zetasizer (Malvern Inst., UK; Nano ZS Zetasizer) (32).

pH measurement. The pH is a crucial determinant of the ionic interaction between pluronic F-127 and the gold NP surface, and thus of loading efficiency. The pH values of formulations were measured using a digital pH meter (Hanna Instrument HI 9321, Ann Arbor, MI) and adjusted to 6.0 using 0.01 M NaOH.

Drug loading efficiency. The theoretical %DL was calculated as the ratio of 5-FU loaded to the total initial amount used in the formulation (Eq. 1).

Drug loading (%)

$$= \text{(Drug content in coated polymer/total drug in NPs)} \times 100 \tag{1}$$

Each formulation (5 mL) was subjected to ultracentrifugation (22,000g) for 20 min. The supernatant (1 mL) was removed and analyzed for free 5-FU using a UV-Vis spectrophotometer at 262 nm. Measurements were conducted in triplicate, and the means and standard deviations (SD) were obtained for analysis.

In vitro drug release. Cumulative drug release from the drug solution (DS) and formulations were assessed using a dissolution Apparatus-II (Paddle). The samples were transferred to a dialysis membrane (12–14 kDa molecular cutoff), which was then tied at both ends and placed inside a stainless steel spiral sinker. The dialysis was conducted under constant paddle stirring (50 rpm) and temperature ($37 \pm 1°C$) in 900 mL PBS pH 7.4 as the release medium (33). To estimate the drug released at each sampling time point (1, 2, 3, 4, 5, 6, 7, 8, 9, 10, 11, 12, 24 and 48 h), a constant volume of the sample (1 mL) was withdrawn and subsequently replaced with fresh dissolution medium. The removed sample was first filtered using a membrane filter (0.22 μm) and then centrifuged (12,000 rpm for 15 min). The concentration of released 5-FU was determined using a spectrophotometer at 262 nm (λ_{max}) (34). The kinetics of the drug released from the formulations were assessed using various mathematical models.

Hydrophilic 5-FU should be readily released from the pluronic matrix into media. Several mathematical models (zero-order, first-order, Higuchi, and Korsemeyer–Peppas) were used to assess the release kinetics (35). Zero-order kinetics were modeled using Eq. (2):

$$C_t = C_0 + K_0 t \tag{2}$$

where C_t is the quantity of 5-FU released at time t, C_0 is the initial concentration of 5-FU at time $t = 0$, and K_0 is the zero-order rate constant.

First-order release kinetics were modeled using Eq. (3):

$$dC/dt = -K_1 C \tag{3}$$

where C_o is the original concentration, dC/dt is the rate of release, and K_1 is the first order rate constant (expressed per hour). Model fit was then evaluated from the coefficient of multiple determination ($0 \leq r^2 \leq 1$) (35).

The Korsmeyer–Peppas model is defined as

$$M_t/M_\infty = Kt^n \tag{4}$$

where M_t/M_∞ represents the fractional of the drug released at time t, whereas k and n indicate the release rate constant and release exponent, respectively.

Similarly, the Higuchi model was applied and a plot was presented using the % cumulative DR as function of square root of time. Mathematically, it was defined as Eq. (5):

$$Q = Kt^{1/2} \tag{5}$$

where Q represents the cumulative percent drug released over time, t and K is a release rate constant.

Optimization Using Experimental Design Software (Design Expert®)

Based on the preliminary findings (particle size, PDI, ZP, and DL efficiency), it was important to optimize an optimum concentration of gold salt (250–500 mg/L) and CLS concentration (10–100%). Drug content and the amount of pluronic F127 were kept constant. This would provide a robust formulation with optimum size, maximum 5-FU %DL, ZP, and % drug release (%DR). A full factorial design with two factors and three levels (3^2) against four responses were run with a zero central point using Design Expert® software (version 8.0.7.1, Stat-Ease, Inc., Minneapolis, MA). Gold salt and the CLS were two independent factors defined as X_1 and X_2, whereas particle size formulations (Y_1, nm), %DL (Y_2, %), ZP (Y_3, mV), and %DR (Y_4, %) were variables tested. Three levels of X_1 and X_2 were represented as "+ 1," "0," and "− 1" for maximum, intermediate, and lower values, respectively. Polynomial mathematical equations were generated for each response, and statistical calculations were carried out to identify prime factors affecting the responses and the interactions between X_1 and X_2. The linear equation was represented as $Y = B_0 + AX_1 + BX_2$, where B_0, A, and B were the intercept, linear coefficient for X_1, and linear coefficient for X_2, respectively.

Finally, a desirability objective function was applied to obtain individual and overall desirability. This is a numerical objective function (between zero to 1) to validate the model and identify interactions. The value near 1 indicated the best fit of the model whereas a lower value represented a poor fit of the model. A zero value meant out of fit of the model. The value obtained depended on the number of responses taken into analysis and the set constraints (within range, targeted, minimum, and maximum). The importance given to the particular response (Y) changes the overall desirability function (36).

Evaluation of Optimized Formulations

Chemical interaction measurements using the FTIR spectral analysis. To assess possible chemical interactions between drugs and gold in the NPs, a FTIR spectral study was performed using the conventional potassium bromide (KBr) disc method (Shimazdu FTIR 8400S). Individual formulations were completely blended with solid KBr and transformed into a pellet (1:10). The infrared (IR) absorption spectra of 5-FU, pluronic F-127, PLGA, gold salt (auric acid), placebo, and corresponding drug-loaded formulations were examined by scanning in the range 4000–500 cm^{-1}. The spectra were then analyzed for the characteristic peaks of drug-auric acid conjugates.

Morphological assessment of biogenic gold NPs and PLGA NPs. To investigate morphological shape and size of the NPs, transmission electron microscopy (TEM) (Tecnail 2, 120KV, FEI Company, Eindhoven, The Netherlands) was used. The sample (100-fold diluted with distilled water) was dropped over a previously prepared carbon film-coated copper grid and stained with negative staining agent (2% w/v, phosphotungstic acid) followed by drying overnight at ambient temperature (25°C). In case of excess sample, a non-shedding filter paper was used to remove any excess from the grid. The particles were visualized under TEM at various magnifications and resolutions.

Cytotoxicity

Cell lines and growth media. The cytotoxicity of the different formulations was tested against human colon cell lines. Briefly, cells were seeded in 75-mL culture flasks and maintained in DMEM supplemented with 10% fetal bovine serum (FBA) (Gibco, USA) plus 5 mg/mL antibiotic/antimycotic solution under standard conditions (18% O_2 and 5% CO_2 at 37°C). At confluence, cultures were split using 0.25% trypsin-ethylenediaminetetraacetic acid (EDTA) solution (HiMedia) and seeded in culture plates for drug treatment. Treatments were conducted 72 h later at ~ 70–80% confluence.

MTT cell viability assay. Cell toxicity induced by each formulation was evaluated using the 3-(4,5-dimethylthiazol-2-yl)-2,5-diphenyltetrazolium bromide (MTT) assay, which estimates the number of remaining viable cells based on the capacity of functional mitochondria to convert tetrazolium salt to purple formazan crystals (33). The cell line was seeded at 5×10^3 cells/well in sterile 96-well plates, cultured for 24 h, and then exposed to the indicated formulation for 4, 8, 12, and 24 h. A 20 μL volume of MTT solution (5 mg/mL) was then added to each well and culture continued for an additional 4 h. The medium was then removed and 100 μL of dimethyl sulfoxide (DMSO) was added to dissolve the accumulated formazan. Formazan generation (proportional to the number of viable cells) was measured using an ELISA reader (BioRad) at 490 nm. Percent relative cell viability was calculated according to the equation:

%Relative cell viability

$$= (\text{OD of test sample}/\text{OD of control sample}) \times 100 \quad (6)$$

where the OD is an optical density at 490 nm.

In Vitro Hemolysis

Hemolysis was carried out following the reported method with slight modification (37). Erythrocytes from a healthy volunteer were suspended in PBS (4% v/v) and treated with the indicated formulation for 4 h at 37 ± 1°C. All the formulations (PNPs, GNPs, PFNPs, FGNPs, and OBPN-1) were freshly prepared and sterilized immediately before experiments. Distilled water and saline served as positive and negative controls, respectively. Briefly, 2 mL PBS was combined with 0.5 mL of the indicated formulation and 0.5 mL of erythrocytes suspension and mixed gently. The mixture was centrifuged and the concentration of released hemoglobin in the supernatant was estimated using a UV-Vis spectrophotometer at λ_{max} of 540 nm. Percent hemolysis was calculated as

$$\text{Percent hemolysis} = [(A_S - A_N)/(A_P - A_N)] \times 100 \quad (7)$$

where A_s, A_N, and A_P are the absorbance values of the test sample, negative control, and positive control, respectively. Hemolysis caused by the positive control was set to 100%.

Ex Vivo Permeation Across the Intestinal Tissue

NPs were examined for permeation across the rat intestine (duodenum, ileum, and jejunum). These experiments were approved by the Institutional Ethics Committee and conducted as described in ARRIVE guidelines (LDH/IAEC/1370) (34). Briefly, the rat small intestine was excised, cleaned, and cut into 2-cm segments. Segments were loaded with 1 mL of the indicated formulation (containing about 10 mg of drug) and tied at both ends. The tissue was then placed in a modified USP dissolution apparatus maintained at constant temperature (37 ± 1°C) with appropriate aeration and paddle speed. A 500 mL of PBS (pH 7.4) was used as the release medium. The release medium was sampled at 1, 2, 4, 8, 12, 16, 20, and 24 min, and each sample was immediately

replaced with fresh release medium. The protocol and procedure were followed as per the reported method with slight modification (38). The amount of 5-FU permeated across the intestinal wall was estimated using a UV-Vis spectrophotometer.

Statistical Analysis

Cytotoxicity and release kinetics are expressed as mean and SD. Cytotoxicity was compared by Student's t test. A $p < 0.05$ (two-tailed) was considered significant. All of the studies were performed in triplicate to obtain mean and SD.

RESULTS AND DISCUSSION

Preparation of NP Formulations

Placebo NPs (PNPs, GNPs, and PGNPs) and 5-FU-loaded formulations (PFNPs, FGNPs, and PFGNPs) were prepared and evaluated for particle size, PDI, ZP, %DL, and pH (Table 1). Gold NPs were prepared biogenically using the bacterial extract containing synthesis enzymes and capped with pluronic F-127 for stability and surface functionalization. PLGA-based NPs were compared with pluronic-capped gold NPs. PLGA has a well-documented biosafety and biocompatibility profile in various drug delivery and commercial products. Here, we show that the pluronic surface coating (a) increased DL efficiency, (b) increased ZP, (c) enhanced biocompatibility, (d) slightly increased the particle size due to the surface coating, and (e) exhibited an anticipated improved cytotoxic efficacy against cancer cells. Pluronic-coated PFGNPs presented the following particle size, PDI, ZP, and %DL values: 178.21 ± 10.62 nm, 0.202, -29.32 ± 0.26 mV, and $93.09 \pm 10.75\%$, respectively. Placebo gold NPs and polymeric NPs (PLGA) had lower particle size and PDI as shown in Table 1. Moreover, the %DL of the PFGNPs was remarkably higher than polymeric PFNPs (~ 67.68%) and FGNPs (~ 72.0%), which may be due to the interaction of 5-FU with the gold core surface and entrapment between the pluronic coating and the gold surface. Moreover, the pluronic coating improved the NP stabilization and drug retention onto the adsorbed surface (12). There are several potential factors such as gold salt and extract concentrations that affect the gold NPs size, shape, %DL, %DR, and surface charge (39). Therefore, we needed to optimize the CLS content and gold salt concentration to obtain robust gold NPs with optimized size, ZP, %DL and %DR over a 12-h period.

pH Measurement

The final pH values of all formulations were adjusted to ~ 6 as this maximized the interaction between 5-FU, pluronic, and gold core surfaces. 5-FU possesses two pKa values of ~ 8.0 and ~ 13 due to the presence of an amino group, and achieves full ionization at pH 6. Protonation of the amino group in 5-FU is essential for its incorporation into drug delivery systems, particularly polymeric and gold-based NPs (40–42). The pH dictates the degree of ionization, the strength of the ionic interaction between the pluronic and gold NPs, DL efficiency, drug release behavior, particle aggregation, and stability. 5-FU is anionic at pH   6.0;

therefore, loading is less efficient and stability is poorer at lower pH values (25). Moreover, the pKa determines the pH dependence of drug release, which is important as tumor tissue has a lower extracellular pH than normal tissue (43). Both 5-FU and the pluronic coating are completely ionized at pH 6.0, which may create a strong ionic interaction for efficient DL (42).

Optimization and Desirability Function

The experimental design tool constituted to identify the independent variables (factors), their levels, and their relative importance during the "optimization process." This helped to select important factors affecting responses and excluding non-significant factors in the optimization process. The tool also helped to identify possible interactions between factors. The independent factors (X_1 and X_2) and their levels (three as maximum, intermediate, and minimum, 3^2) were selected based on the cellular enzyme concentration (diluted and undiluted) and gold salt (auric salt), which are the main components affecting the physicochemical properties of gold NPs during biogenic synthesis (Table 2) (39). Lower concentrations of gold salt and diluted CLS are responsible for smaller particle size (30–80 nm) at 30°C (39).

Particle size: Y_1. Particle size is one of the strongest factors influencing drug delivery because it directly impacts on formulation stability, access to the lymphatic system (which improves oral absorption), and preferential passive accumulation in tumor tissue (44, 45). Measurements of particle size, PDI, and ZP are presented for all formulations in Table 1. As expected, pluronic-coated PGNPs were significantly larger than uncoated GNPs (173.2 ± 6.71 nm *vs.* 29.11 ± 1.01 nm). Furthermore, FGNPs were also larger than GNPs, in agreement with the red shift values and the suggested substantial 5-FU loading values (12, 46). Both polymeric (PNPs and PFNPs) NPs exhibited moderate variation in particle size (118.91 ± 3.12 nm and 98.29 ± 5.42 nm, respectively). DL of GNPs resulted in a slight increase in the PDI (from 0.191 to 0.271) and was associated with similar size distribution (0.292 and 0.271, respectively). Similarly, the pluronic coating increased the particle size of gold-based NPs (from FGNPs 159.81 ± 6.28 nm to PFGNPs 178.21 ± 11.62 nm). Overall, the particle size distribution of the PFGNPs was the narrowest, again consistent with the PDI findings.

The particle size of the nanocarrier formulations is a critical factor for stability, efficient delivery, and drug targeting to the tumor site. Placebo gold NPs exhibited negative ZP (-11.19 mV), which facilitated surface functionalization with the pluronic coating. Thus, both the drug adsorption and surface functionalization are responsible for surface neutralization and the increment in the NPs size, respectively as evidenced by the significant reduction in the ZP of FGNPs (-8.52 mV and size of 159.81 nm) as compared with GNPs (-11.19 mV and size of 29.11 nm) (46). The pluronic coating on gold NPs had a stabilizing effect without deliberately affecting the particle size distribution determined by the PDA) (Table 1). Particle size and surface charge (ZP) greatly affect the stability of NPs, *in vitro* behavior, *in vivo* performance, and biodistribution (47).

Table 1. Preliminary Study of Polymeric and Biogenic Gold NPs for Selection of Independent and Dependent Factors

Sample	Particle size (nm)	PDI	Zeta potential (mV)	DL (%)	Final pH
GNPs	29.11 ± 1.01	0.292	−11.19 ± 0.81	–	6.1
PNPs	118.91 ± 3.12	0.191	−29.11 ± 0.18	–	6.0
PFNPs	98.29 ± 5.42	0.271	−28.76 ± 0.39	67.68 ± 7.74	6.1
PGNPs	173.2 ± 6.71	0.249	−22.92 ± 0.32	–	6.2
FGNPs	159.81 ± 6.28	0.281	−8.52 ± 0.29	71.91 ± 11.86	6.1
PFGNPs	178.21 ± 10.62	0.202	−29.32 ± 0.26	93.09 ± 10.75	6.1

PDI polydispersity index, *DL* drug loading efficiency, *GNPs* placebo gold NPs, *PNPs* PLGA-based NPs, *PGNPs* pluronic-coated gold NPs, *FGNPs* 5-FU-loaded gold NPs, *PFGNPs* pluronic-coated drug-loaded gold NPs, *PFNPs* 5-FU-loaded PLGA coated NPs

The generated mathematical polynomial equation of the response Y_1 is expressed by the linear equation $Y_1 = 137.46 + 33.22X_1 + 78.75X_2$. In general, the positive and negative signs of terms indicated synergistic and antagonistic effects between factors and respective dependent variables (responses). In this equation, the relationship between factors and response is synergistic, which means that the particle size was directly proportional to the concentration of the factors X_1 and X_2. Thus, an optimum size (200 nm) can be achieved by reducing the concentration of gold salt and CLS. The higher values of F ($F = 247.58$) and p ($p = 0.0001$) represented the reliability of the best fit of the model between factors and dependent variables (Table 3). Predicted and adjusted regression coefficient (r^2) values were 0.9709 and 0.9840, respectively, which showed the reliability and the best fit of the model (linear) in optimization process. The regular "r^2" was 0.9980 (Table 3). Thus, the particle size was between 30.2 and 258.5 nm (Table 2). The system generated the three-dimensional surface and contour plots shown in Fig. 1 a and b, respectively. Both plots suggested there was a linear relationship between factors and Y_1. The software suggested two optimized formulations, OBPN-1 ($X_1 = 500.0$ mg/L and $X_2 = 77.6\%$ diluted CLS) and OBPN-2 ($X_1 = 500.0$ mg/L and $X_2 = 76.11\%$ diluted CLS), under the set constraints and relative importance (Table 3). Both predicted (172.4 nm) and experimental (185.1 nm) values were in close agreement with the best fit of the model (Table 3 and Fig. 2a). Thus, an optimized formulation may be achieved using higher concentrations of gold salt (500 mg/L) and 78% diluted CLS to achieve the desired goals.

Percent drug loading (%DL): Y_2. The pluronic-coated PFGNPs exhibited substantially greater loading efficiency (%DL) that either PFNPs or FGNPs (93.09% ± 10.75% *vs.* 67.68% ± 7.74% and 71.91% ± 11.86%) (Table 1). However, all these values were substantially higher than the synthetic

Table 2. Combination of Levels and Independent and Dependent Variables for PFGNPs Loaded with 5-FU (100 mg)

Independent variables	Levels					
	Low		Middle		High	
	Coded	Actual	Coded	Actual	Coded	Actual
X_1: Gold salt (mg/L)	−1	250	0	375	+1	500
X_2: CLS (%)	−1	10	0	55	+1	100
			Constraints			
Dependent variables		Low	High	Goal	Model	
Y_1: size (nm)		30.2	258.5	In range	Linear	
Y_2: %DL		10.2	95.3	Targeted	Linear	
Y_3: zeta potential (−mV)		11.4	34.7	In range	Linear	
Y_4: %DR		10.3	98.5	Targeted	Linear	
Combination levels of independent variables and their responses						
Formulation code	X_1	X_2	Y_1	Y_2	Y_3	Y_4
BPN1	(−1)	(−1)	30.2	10.2	−18.2	19.3
BPN2	(0)	(−1)	63.8	28.7	−16.1	25.1
BPN3	(+1)	(−1)	79.5	39.5	−11.4	31.7
BPN4	(−1)	(0)	98.5	21.7	−22.1	45.9
BPN5	(0)	(0)	149.3	47.8	−20.1	59.4
BPN6	(+1)	(0)	169.5	69.7	−19.2	70.8
BPN7	(−1)	(+1)	179.1	35.5	−34.7	58.7
BPN8	(0)	(+1)	208.4	71.1	−30.2	78.9
BPN9	(+1)	(+1)	258.5	95.3	−28.2	89.5

Table 3. Summary of Statistical Analysis (3^2 Factorial Design)

Coefficients	Responses			
	Y_1	Y_2	Y_3	Y_4
B_0	137.46	46.61	22.22	54.25
B_1	33.21	22.85	2.733	12.85
p value	0.0001	0.0002	0.012	0.003
F value	74.79	69.31	12.52	21.38
B_2	78.75	20.58	7.9	26.66
p value	0.0001	0.0003	0.0001	0.0001
F value	420.37	56.23	104.65	92.099
Model statistics				
r^2	0.9980	0.9943	0.9812	0.9969
Adjusted r^2	0.9840	0.9791	0.9751	0.9830
Predicted r^2	0.9709	0.9586	0.9570	0.9672
Model F value	247.58	62.72	58.58	56.74
Model p value	0.0001	0.0001	0.0001	0.0001
% CV value	6.84	14.42	8.51	12.54
	Observed/(predicted) values			
Optimized	Y_1	Y_2	Y_3	Y_4
OBPN-1	175.1 (172.4)	73.8 (79.79)	21.8 (23.45)	75.7 (80.50)
OBPN-2	171.7 (173.9)	71.2 (79.11)	20.7 (23.19)	82.1 (79.11)

Polynomial equations for each response
$Y_1 = 137.46 + 33.22X_1 + 78.75X_2$
$Y_2 = 46.61 + 22.85X_1 + 20.58X_2$
$Y_3 = 22.22 - 2.733X_1 + 7.9X_2$
$Y_4 = 54.25 + 12.85X_1 + 26.66X_2$

$Y1$ = particle size; $Y2$ = %DL (drug loading); $Y3$ = zeta potential; $Y4$ = %DR (drug release); $r2$ = regression coefficient; % CV = percent coefficient of variation

methods using two different surface functionalizing agents (20.96% and 29.34%) (12). The biogenic NPs possessed a protein corona with catalytic activity that served as an effective host for the substrate (48). The absolute difference compared with previous studies may thus be attributed to the catalytic activity of the biogenic GNPs and the strong electrostatic interactions between the protonated amino group of 5-FU (cationic) and the negatively charged pluronic coating at pH 6 due to the carboxylic acid groups (*i.e.*, the amino acid in the enzyme protein sequence) (49). At pH > 6, the positive charge intensity of 5-FU was reported to decrease owing to the deprotonation of the amino group, resulting in decreased %DL, while at pH < 6, the ionization of the carboxylic group decreased, further reducing the %DL due to the weaker ionic interaction with the drug (12). However, PFGNPs demonstrated the highest %DL, possibly due to the preferential adsorption of 5-FU by the hydrophilic biogenic GNP surface and stronger electrostatic interaction amongst the drug, pluronic coating, and gold surface at its fully ionized pH. That is, hydrophilic 5-FU was efficiently impregnated in the pluronic matrix already coated on the gold core for highly efficient DL, while the gold core provided additional stability and uniform particle size.

In the preliminary results, the pluronic coating improved the 5-FU loading efficiency (93.09%) as compared with polymeric PLGA-based NPs (Table 1). The drug is hydrophilic and shows poor membrane permeability, which may be increased by loading onto the GNPs and subsequent capping with the pluronic coating to improve stability (12, 50).

Loading of hydrophilic drugs is inefficient on chemically synthesized hydrophobic GNPs. Indeed, the loading of 5-FU was reported as only ~ 2% at pH 6.0, which is below the theoretical limit (12, 51). However, our findings revealed ~ 72.0% DL was achieved, which may be due to the biogenic gold core surface interacting with hydrophilic surface, which allowed a better adherence of the polyphenol compound. 5-FU bears an amino group (pKa ~ 8.0) and enzymes possess several carboxylic groups. These two groups may be responsible for the ionic interactions leading to improved DL at pH 6.1, as amino group protonation is required for 5-FU loading in drug delivery systems (39, 52). Furthermore, the pluronic coating stabilized and improved the DL to 93.09%. The %DL values were found to be in the range 10.2–95.03 (Table 3).

The generated polynomial linear equation for %DL was $Y_2 = 46.61 + 22.85X_1 + 20.58X_2$. Both terms involved positive sign suggesting a synergistic effect by X_1 and X_2 on the dependent variable Y_2. The higher values of F ($F = 62.72$) and p ($p = 0.0001$) corroborated the best fit of the model. The adjusted and predicted r^2 values were found to have 0.9791 and 0.9586, respectively, whereas regular r^2 was 0.9943 (Table 3). The regression coefficient ensured the best fit of the model during the optimization process. The 3D surface and 2D contour plots are shown in Fig. 1 c and d. Similarly, the predicted and observed values of %DL (Y_2) are in close agreement with each other as shown in Table 3 and Fig. 2b, respectively. The linear model suggested that the smaller-sized optimized formulation can be obtained by reducing the concentrations of X_1 and X_2. To
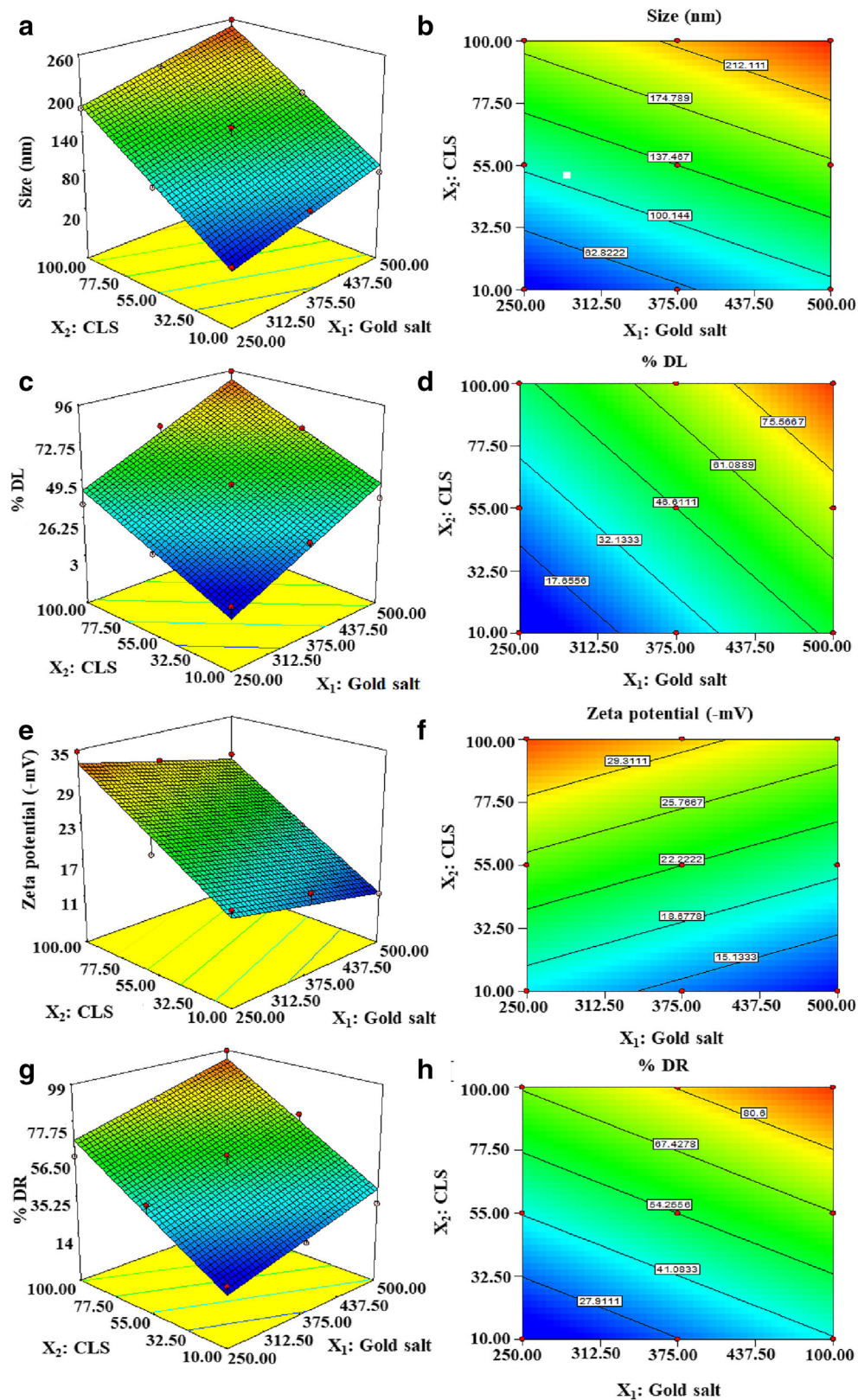
Fig. 1. Three-dimensional response surface and 2D contour plots of four responses: **a** particle size (Y_1), **b** %DL (Y_2), **c** zeta potential (Y_3), and **d** %DR (Y_4)

maximize the interactions between the drug and gold NPs surface, the final pH was kept at 6.1. Other parameters such as temperature and volume were constant in this study.

Zeta potential: Y_3. The surface ZP is an index of inter-particle electrostatic repulsion and thus, is predictive of formulation stability. NPs with ZP values above 30 mV or
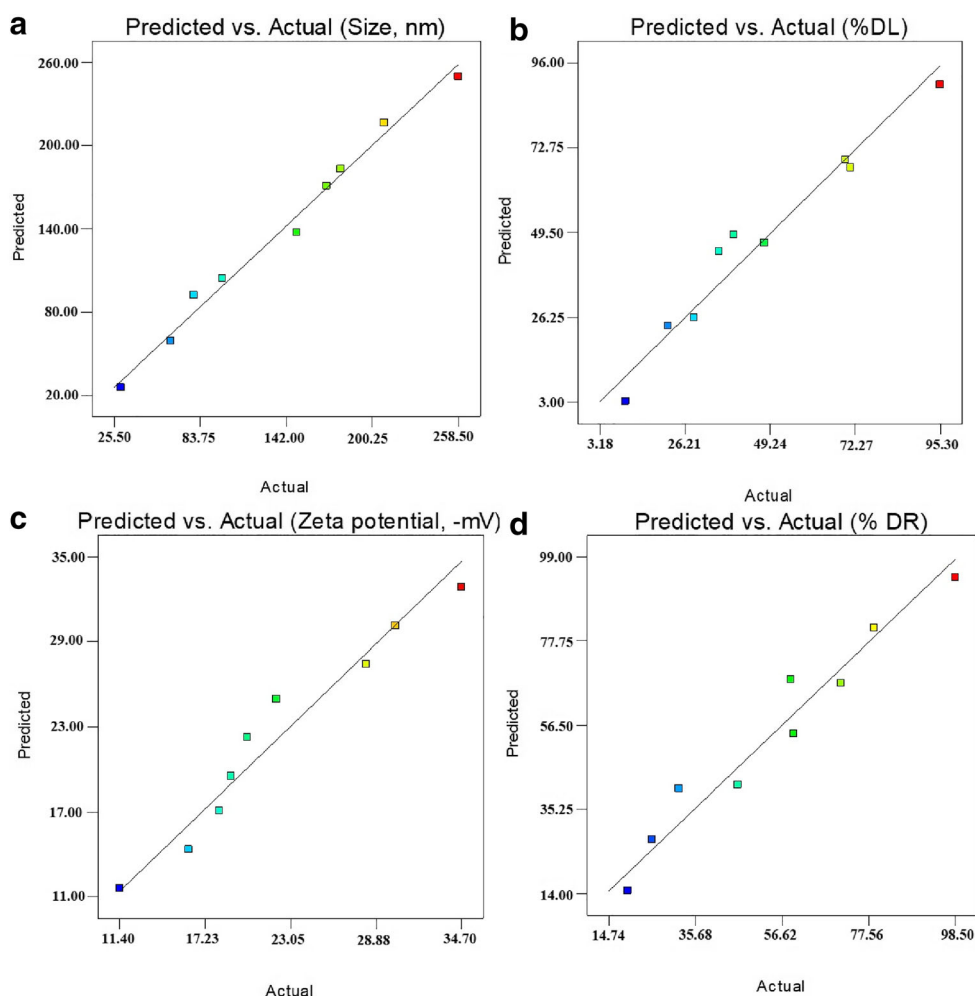
Fig. 2. Predicted and actual plots and their relationship generated from Design Expert: **a** particle size (Y_1), **b** %DL (Y_2), **c** zeta potential (Y_3), and **d** %DR (Y_4)

below − 30 mV typically possess high electrostatic repulsion, resulting in greater colloidal stability (53). The ZP values of all of the preliminary formulations are summarized in Table 1. The GNPs and FGNPs exhibited the smallest values (− 11.19 mV and − 13.52 mV, respectively), possibly because the positively charged Au in these Au-based biogenic NPs acts as a reducing agent. All of the polymeric (PLGA)-based formulations possessed negative ZP values, which may reflect the chemical nature of PLGA and of the biosynthetic enzyme. Pluronic is an amphiphilic block polymer possessing hydroxyl end groups responsible for the hydrophilicity and negatively charged ZP (54). The pluronic-coated PFGNPs had the highest ZP (− 29.71 mV), possibly due to the uncapped terminal hydroxyl and carboxylic groups on the NP surface and the chemical nature of the enzyme adhering on the surface (Table 1). All formulations containing PLGA possessed relatively high ZPs (surface charge) and thus, are likely to be more stable than the other formulations (Table 1). Higher values of ZP for the formulations coated with PLGA may be attributed to more acidic nature (free carboxylic acid as end groups of PLGA) of PLGA and its monomer as degradation product in aqueous phase. PLGA is slowly degraded (hydrolysis) in aqueous medium and is responsible for higher ZP after assessment. Thus, pluronic-coated

formulations were relatively stabilized with optimum values of ZP with considerable stability in aqueous medium. Pluronic has considerable impact on the particle size and ZP of the nanoparticles. It is accumulated on the surface of gold core, and this phenomenon is attributed to the increase of polymers chain numbers per unit volume which results in a bulky structure and larger particle size as evidenced in Table 1 (55). Nanoparticles without PLGA has less negative ZP value (− 8 to − 11 mV) due to cellular enzyme-based coating over the gold core. On the other hand, PLGA or pluronic-based coating increased negative Z p values (− 30 mV) which may be prudent to correlate with significant accumulation of both polymer onto the surface.

Particle size and ZP are responsible for stability and the *in vitro–in vivo* activity. Thus, pluronic capping was carried out on the synthesized biogenic gold NPs. The blank GNPs surface charge carried less negative charge (Table 1). Observed values of ZP (nine formulations) ranged from − 11.3 to − 34.7 mV (Table 2). The generated polynomial linear equation was $Y_3 = 22.22 - 2.733X_1 + 7.9X_2$, which includes positive and negative terms. The optimized formulation could be tailored by reducing the concentration of gold salt (X_1) and increasing the concentration of CLS (X_2) as shown in Tables 2 and 3. The higher values of F ($F = 58.58$) and p ($p =$
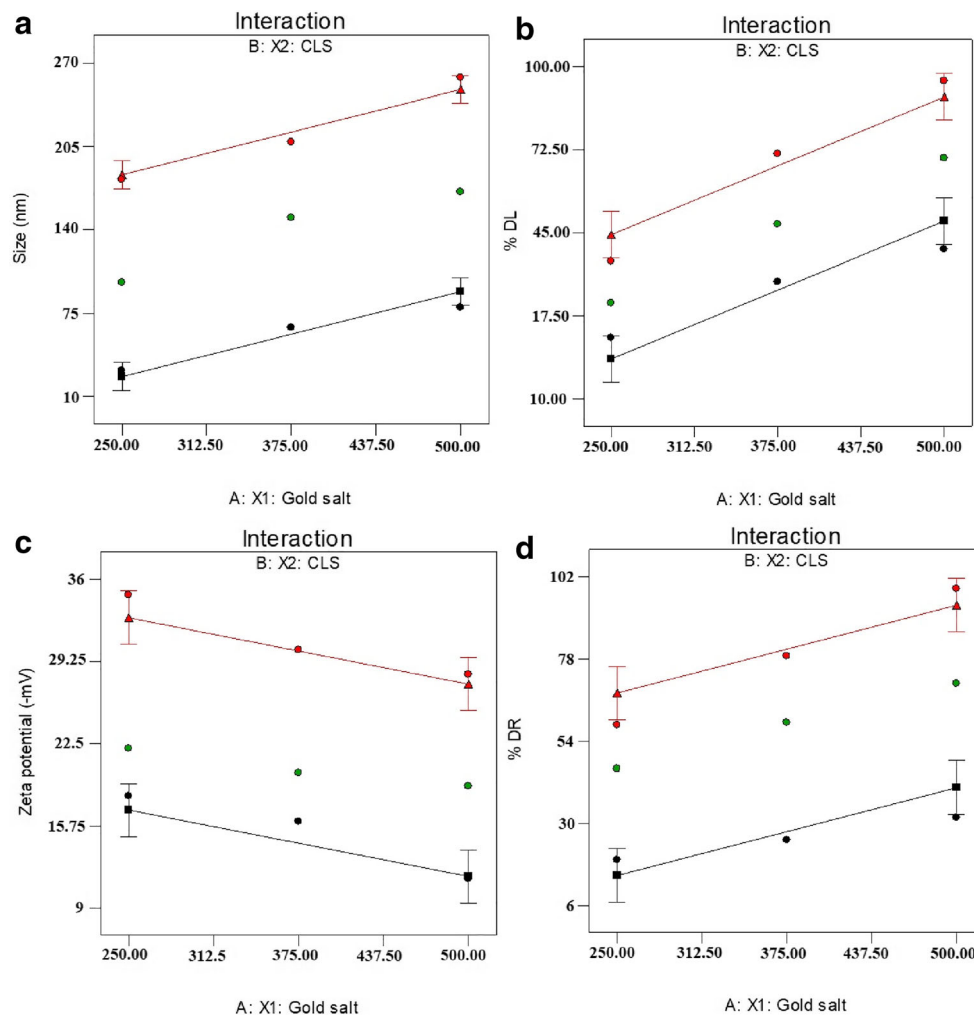
Fig. 3. Interaction curves generated from Design Expert: **a** particle size (Y_1), **b** %DL (Y_2), **c** zeta potential (Y_3), and **d** %DR (Y_4)

0.0001) suggested the best fit of the model and of the optimization process. This was further supported by closely related values of predicted and adjusted values of r^2 (Table 3). The 3D surface and 2D contour plots of Y_3 are shown in Fig. 1 e and f, respectively. Similarly, the predicted and observed values confirmed the best fit of the model with their close values and graphical representation (Fig. 2c). There were no interactions between factors (X_1 and X_2) for the responses (Fig. 3).

% Drug release: Y_4. The mechanistic details of 5-FU release from the PLGA matrix and pluronic-coated GNPs have been described previously (12, 56). *In vitro* 5-FU release from several PLGA-based formulations follows biphasic or triphasic kinetics. Therefore, release may be diffusion-mediated or mediated by a combination of diffusion and erosion. Burst release can be controlled by the high PLGA content in the formulation and pluronic coating over the gold NPs. The cumulative %DR profiles of 5-FU from DS, PFNPs, FGNPs, PFGNPs, and OBPN-1 are shown in Fig. 4. As expected, the DS exhibited the fastest release (82% within 6 h) with no membrane interaction, while the other formulations demonstrated slower and sustained release from the

pluronic-coated OBPN-1 and PFGNPs. The PFGNPs released only about 40% of the loaded 5-FU within 6 h, suggesting a possible sustained release through diffusion from
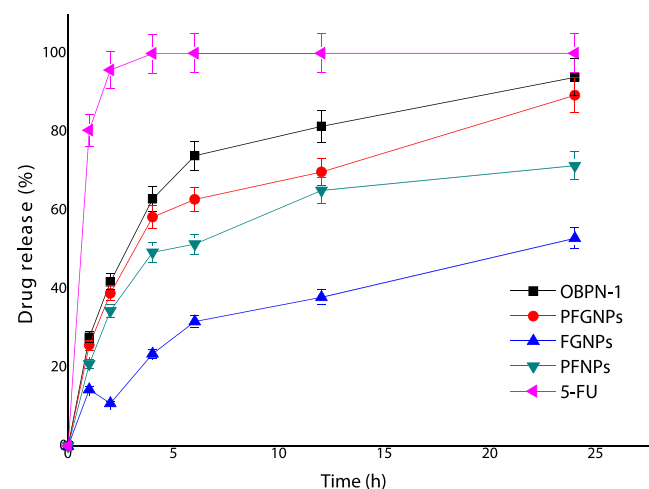

Fig. 4. *In vitro* drug release pattern of 5-FU from various formulation in PBS over period of 24 h

Table 4. Summary Report of *In Vitro* Drug Release Kinetic Models

Models	5-FU solution	PFNPs	FGNPs	PFGNPs	PFGNPs
First-order (R^2)	0.76	0.71	0.74	0.79	0.96
Zero-order (R^2)	0.59	0.99	0.98	0.97	0.99
Korsmeyer–Peppas (R^2)	0.63	0.95	0.97	0.95	0.96
Higuchi (R^2)	0.52	0.98	0.99	0.98	0.98
Hixon–Crowell (R^2)	0.43	0.89	0.96	0.93	0.93
%DR (24 h)	99.9 ± 3.2	71.4 ± 2.9	52.9 ± 5.7	89.3 ± 7.1	96.9 ± 8.05

the matrix (33). In contrast, PFNPs and FGNPs showed a burst release at 60 min, which may indicate faster diffusion from the matrix and a weaker interaction of 5-FU with the GNP gold surface (lower %DL), respectively. The initial burst release (particularly in FGNPs and PFNPs) can be explained by the diffusion of loosely bound 5-FU molecules in the PLGA polymer interior (PFNPs) or weakly adsorbed 5-FU onto the GNP surface (FGNPs). Alternatively, PFGNPs and OBPN-1 exhibited facilitated drug release over the initial 12 h, followed by a sustained release up to 48 h (graph not shown here). These findings are in agreement with earlier reports (45).

Modeling showed that the optimized formulations of FPNPs, FPGNPs, and OBPN-1 all followed zero-order release kinetics, indicating slow and sustained release from the PLGA and pluronic-coated matrix. The %DR are shown in Fig. 4 and the statistical analysis of the various release kinetic models are summarized in Table 4. FGNPs showed a burst release at 1 h, which may be due to weak interaction of 5-FU and the hydrophobic gold core surface (12). Conversely, the pluronic-coated OBPN-1 exhibited a remarkably high (93.3%) and controlled release over a 24-h period. The best fitting model was Higuchi's as indicated by the higher correlation coefficient ($r^2 \geq 0.97$) compared with the other models (Table 4). The drug release kinetics was a critical factor determining the circulating concentration at physiological pH (7.4) and the efficiency of target delivery. As explained above, ionic interactions between 5-FU and the polymer matrix (PLGA and pluronic) are weaker at pH > 6 due to increased deprotonation (12). Thus, two factors may be responsible for the higher release from OBPN-1 compared with PFNPs and FGNPs (Fig. 4): greater DL and favorable release at physiological pH. Early burst release is occasionally desired for DL, while the sustained release reduces the need

for frequent drug administration. This biphasic release of 5-FU from the PLGA-coated GNPs was diffusion attributed ($n = 0.28$) suggesting extended release properties.

Considering physicochemical properties of 5-FU, the drug efficacy can be monitored and improved. In the present study, the solution was maintained at pH 6.1 because the drug is fully ionized and maximally favored for ionic interaction between the gold core surface and 5-FU at explored pH (42). It has been reported that the cation charge intensity on 5-FU decreases due to the deprotonated amino group resulting in decreased %DL and subsequent %DR (12). In the experimental design optimization, a linear polynomial equation was generated and expressed as $Y_4 = 54.25 + 12.85X_1 + 26.66X_2$. Both terms included a positive sign indicating synergistic effects. The optimization process provided "F" and "p" values as 56.74 and 0.0001, respectively, whereas the adjusted and predicted r^2 values were 0.9830 and 0.9672, respectively (Table 3). Thus, the higher value for F and lower value for p produced the best fit of the model during the optimization process for a given set of constraints. The 3D surface and 2D contour plots of Y_4 are shown in Fig. 1 g and h, whereas the predicted and actual values are in close agreement r suggesting good relationship between them (Fig. 2d and Table 3). The optimized formulation can be produced using higher concentration of X_1 and X_2.

The interaction curves for the responses Y_1, Y_2, Y_3, and Y_4 are shown in Fig. 3a–d. The software predicted no possible interaction between factors for each response. Moreover, the overall desirability objective function of the optimized formulations OBPN-1 and OBPN-2 were 0.97 and 0.95, respectively. The individual and overall and individual desirability bar graphs are shown in Fig. 5 a and b for both formulations. The value close to unity validated the best fit of the model in the optimization process and the optimized formulation was obtained within the expected set constraints and relative importance (Tables 2 and 3). The observed
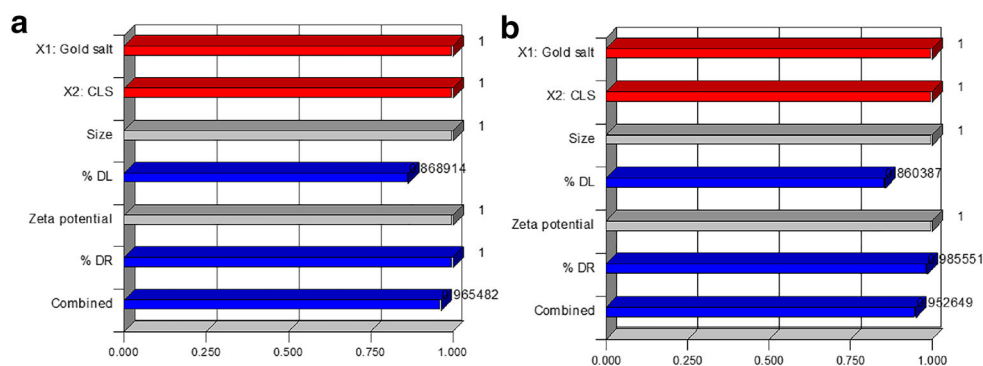
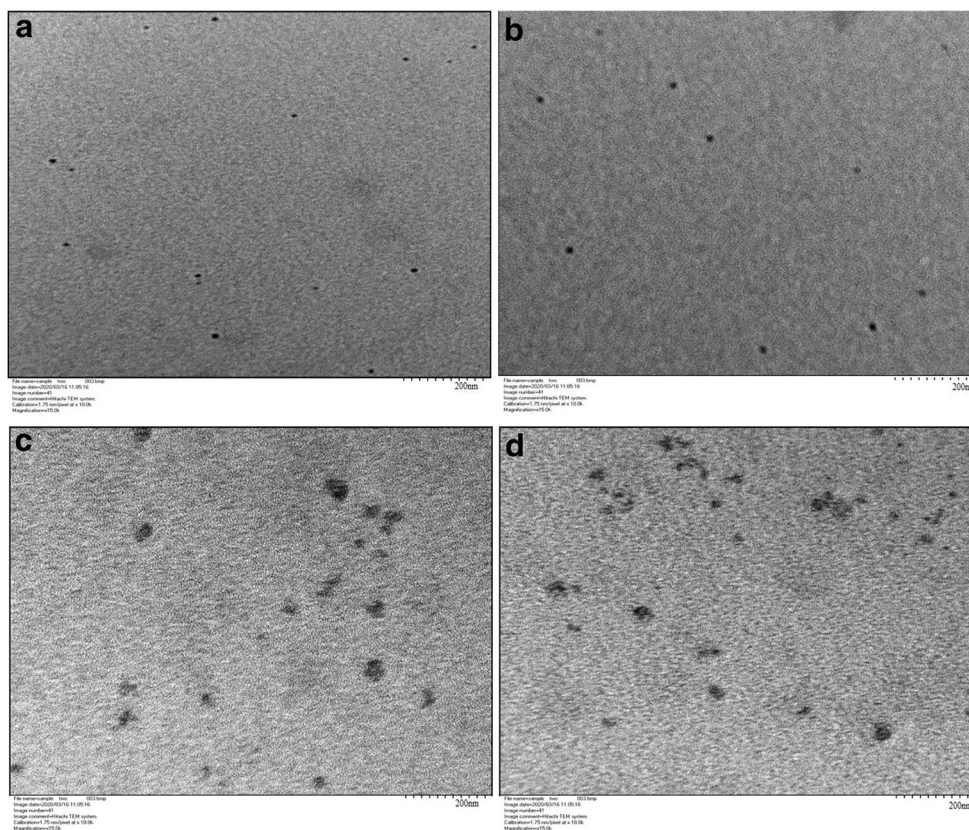**Fig. 5.** Desirability bar graph of optimized formulations: OBPN-1 (**a**) and **b** OBPN-2

Fig. 6. Transmission electron microscopy of polymeric and pluronic-coated gold NPs: **a** placebo GNPs, **b** PLGA based 5-FU-loaded PFNPs, **c** pluronic-coated biogenic 5-FU-loaded PFGNPs, and **d** Finally optimized OBPN-1 with maximum desirability (0.95). Magnification at 150 K

values fall within the two-sided prediction and confidence intervals (95%) of the predicted responses as shown in Table 3.
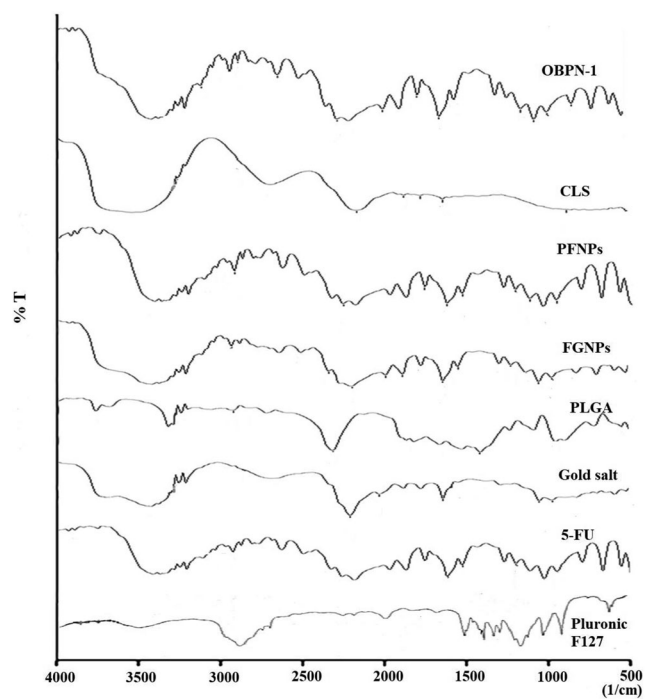
Morphological Analysis

Representative TEM micrographs depicting the spherical structure and surface topography of these NPs formulations are presented in Fig. 6. The GNPs and polymeric PLGA-based PFNPs exhibit homogenous and uniform small-sized distributions (Fig. 6a, b), while the pluronic-coated gold NPs, PFGNPs and OBPN-1, showed relatively irregular surface architecture due to coating and DL (Fig. 6c, d). Figure 6 a reveals a very small and uniformly spherical shape of the placebo GNPs, which is in support of DLS-based particle size analysis. Polymeric-based PLGA NPs also exhibited a similar pattern of size distribution and shape as shown in Fig. 6b. However, the pluronic coating also showed that DL increased the particle size compared with blank formulations, in accordance with previous studies reporting that 5-FU loading onto GNPs caused a slight red shift in the FTIR spectrum (12, 46). Notably, the TEM images clearly confirmed that the size and surface after coating are relatively larger and irregular than the placebo GNPs, respectively. Furthermore, these TEM images demonstrated effective and efficient pluronic-based coating over the reducing gold core, presumably due to the strong negatively charged surface interaction.
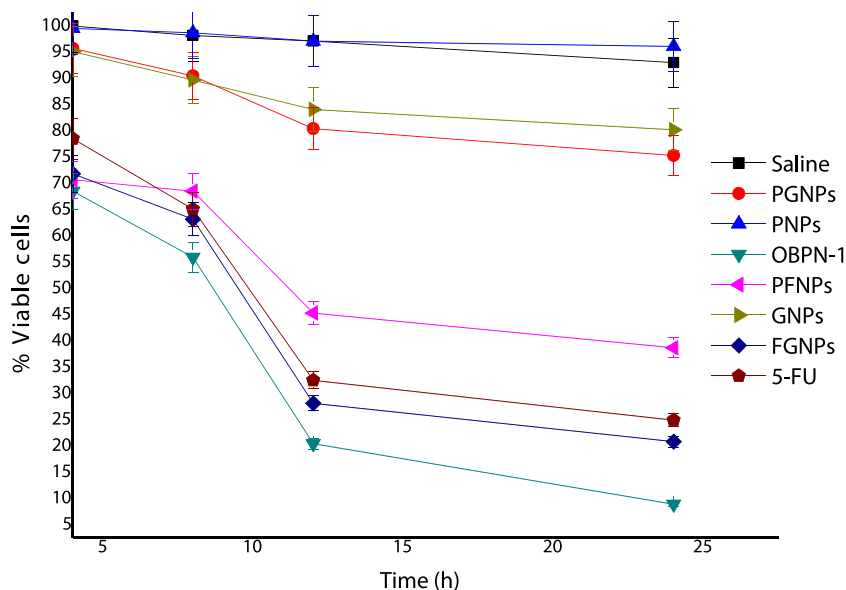

Fig. 7. FTIR spectra of various excipients and pure drug illustrating compatibility of the drug with excipients

Fig. 8. Cytotoxicity study of various formulation and comparison against pure 5-FU at varied time points using colon cancer cell lines (HCT 116)

FTIR Analysis

FTIR spectral analysis was conducted to negate possible chemical interactions between the drug molecule and excipients. The IR absorption spectra of pure 5-FU, the excipients (PLGA, pluronic, and gold salt), placebo (PGNPs), and drug-loaded formulations (FGNPs, OBPN-1 and PFNPs) are shown in Fig. 7. The characteristic peaks of pluronic F-127 are a result of O–H stretching (3485.4 cm^{-1}), C–H aliphatic stretching vibration (2901.5 cm^{-1}), O–H in-plane bending (1342.21 cm^{-1}), and C–O–C stretching (1100.5 cm^{-1}) which are in agreement with reported findings (57). A broad band

between 3066.82 and 3132.40 cm^{-1} in the pure 5-FU spectrum is attributable to –NH stretching vibrations. This band was observed at ~ 3125 cm^{-1} in the IR spectrum of drug-loaded PGNPs. Pure 5-FU also exhibited a band at 1662.64 cm^{-1}, indicative of carbonyl stretching (C=O). A characteristic peak at 1246.02 cm^{-1} in the 5-FU spectrum was attributable to C–F stretching, which was retained in all formulations containing 5-FU, but with a slight red shift. PLGA showed characteristic peaks at 2997.38 cm^{-1} owing to C–H_3, C–H_2 and C–H-based stretching vibrations whereas the bending vibrations revealed characteristic peaks at 1388.75 (1397), 1423.47 (1426), and 1458.91 (1454) cm^{-1} due to the carbonyl (C=O) functional
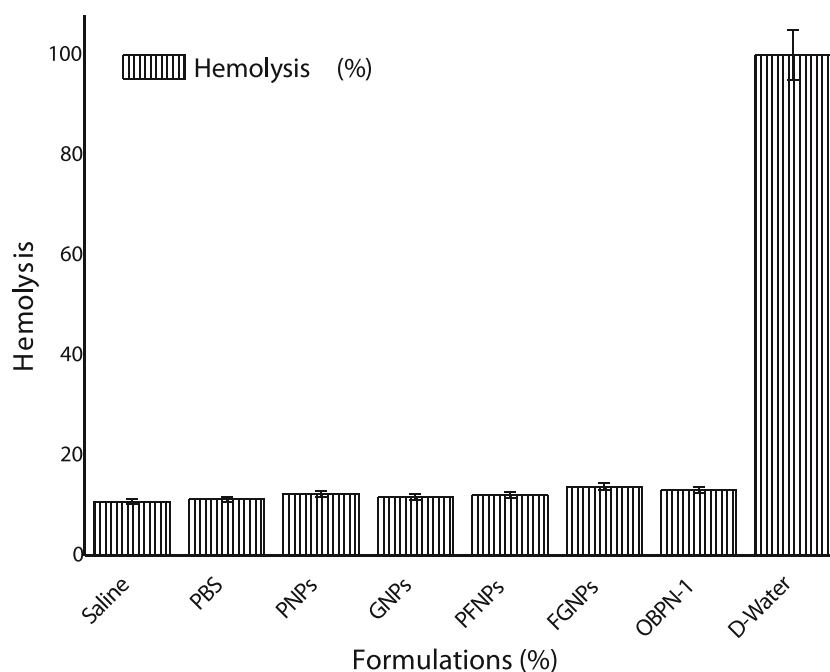

Fig. 9. *In vitro* hemolysis graph exhibiting degree of hemolysis over incubation period of 4 h at 37 ± 1°C

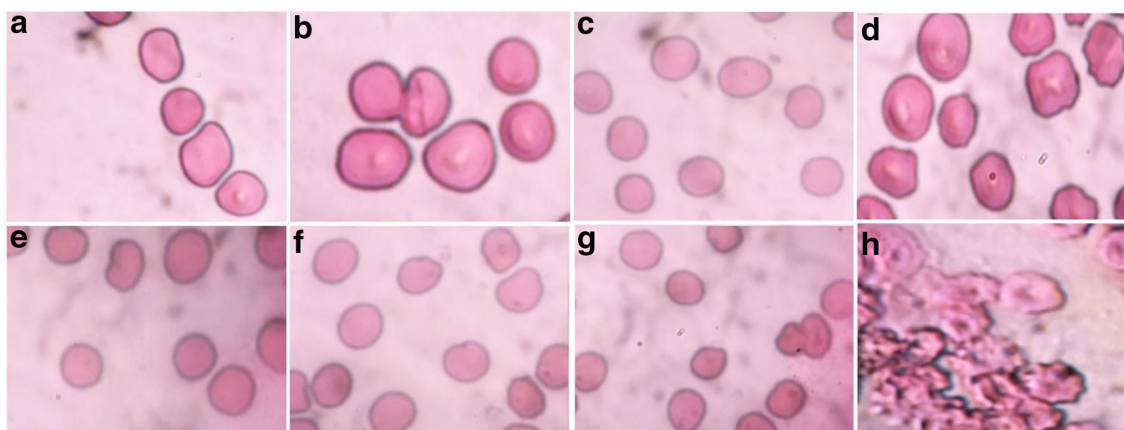**Fig. 10.** *In vitro* hemolysis study of developed formulations for 4-h incubation period at $37 \pm 1°C$. Groups exposed with **a** saline (negative control), **b** PBS, **c** placebo PNPs, **d** placebo GNPs, **e** PFNPs, **f** FGNPs, **g** OBPN-1, and **h** positive control. Red arrow indicated intact human RBCs with apparent margin without any facture or lysis whereas red arrow indicated fractured and lysed cells observed in positive control

group. These peaks are in agreement with previous findings (58). The tetrachloroauric acid (III) as gold salt ($HAuCl_4$) illustrated characteristic peaks at 813.96, 987.55, 1180.44, 1427.32, 1670.35, and 2143.19 cm^{-1} (Fig. 7), wherein a strong vibrational frequency at 1427.32 is related with Au(III) complex formation with chloride. Thus, few characteristic peaks of 5-FU were retained in the formulations (OBPN-1, PFNPs, and FGNPs) suggesting partially impregnated capped polymer, loading over a capped polymer, or free 5-FU without any incompatibility amongst them. The peaks obtained confirmed previous reports describing identity and purity of 5-FU. All characteristic peaks of 5-FU, polymeric NPs and GNPs were obtained in the physical mixture proving absence of any chemical interface between the 5-FU and excipients.

MTT Assay Analysis: Percent Viable Cells

The capacities of these 5-FU formulations to inhibit the proliferation of colon cancer cell lines were examined by the MTT assay (Fig. 8). There were no significant reductions in estimated viable cell number during treatment with placebo formulation (PNPs ~ 96.1%) or saline as the negative control (93.0%) over a period of 24 h. Notably, GNP-treated cultures exhibited a slight reduction in viable cells (GNPs ~ 80.2% and pluronic-coated PGNPs ~ 75.3%), which may be due to gold-induced hyperthermia and the enhanced permeation and retention effects (EPR effect). As suggested by Hirsch et al. (2003), nanoshell treatment increased average tumor temperature by 9°C in mice (59). In contrast, there were significant reductions (p 0.05) in viable cell number with time of exposure to 5-FU solution and to the nanoformulations containing an equivalent amount of 5-FU (Fig. 8). Furthermore, the reduction in viable cell number was remarkably high with OBPN-1 treatment compared with the 5-FU solution (24.9% ± 0.11%) and PFNPs (38.7% ± 0.21%). The pluronic-coated OBPN-1 elicited the greatest cytotoxic effect against the cancer cell line (Fig. 7), which may reflect greater %DL, more efficient pluronic-dependent cellular internalization, increased stability, the gold-based thermal effect, and/or augmented cellular uptake. The small size of the stable gold-based NPs likely enhanced uptake by cancer cells. For instance, ~ 100 nm nanoshells maximally accumulated in breast cancer cells after 24 h of parenteral administration (57). The acidic nature of the tumor extracellular environment may also facilitate internalization as 5-FU is fully ionized under this condition (12). Thus, the conjugate effect of OBPN-1 formulation is relatively superior to the DS and others. This greater cytotoxicity may be attributed to facilitated cellular uptake and high DL.

In Vitro Hemolysis Assessment

Charged molecules, synthetic polymers, the hydrophobic core of gold NPs, and cationic surfactants can induce substantial hemolysis by interacting with the outer leaflet of the red blood cell (RBC) membrane (60). Therefore, we explored the hemocompatibility of excipients, 5-FU, and formulations using rat erythrocytes (Fig. 9). The positive control (distilled water) caused 100% hemolysis as anticipated, whereas the negative control (saline) induced only 11.4% hemolysis over 4 h as measured by the release of hemoglobin into the supernatant. Hemolysis induction by the formulations PFNP (12.6%), FGNP (13.09%), and OBPN-1 (11.8%) did not differ substantially from the negative control or PBS treatment (10.8%), indicating hemocompatibility (37).

As some hemoglobin may be released but is captured in the cell pellet rather than the supernatant, we also examined the extent of RBC lysis in the pellet after re-dispersal in PBS (2 mL). However, few lytic RBCs were observed by light microscopy (400×) in pellets treated with the excipients (Fig. 10b, d) or formulations (Fig. 10e, g) compared with untreated control pellets (Fig. 10a), while most cells were lysed by water treatment (Fig. 10h). Therefore, the nanocarrier appears safe and effective for parenteral, oral, or inhalation drug delivery.

Ex Vivo Permeation Study

The optimized formulations (PFNPs, PGNPs, and OBPN-1) and drug solution (DS) were investigated for permeation (%) across the rat duodenum, jejunum, and
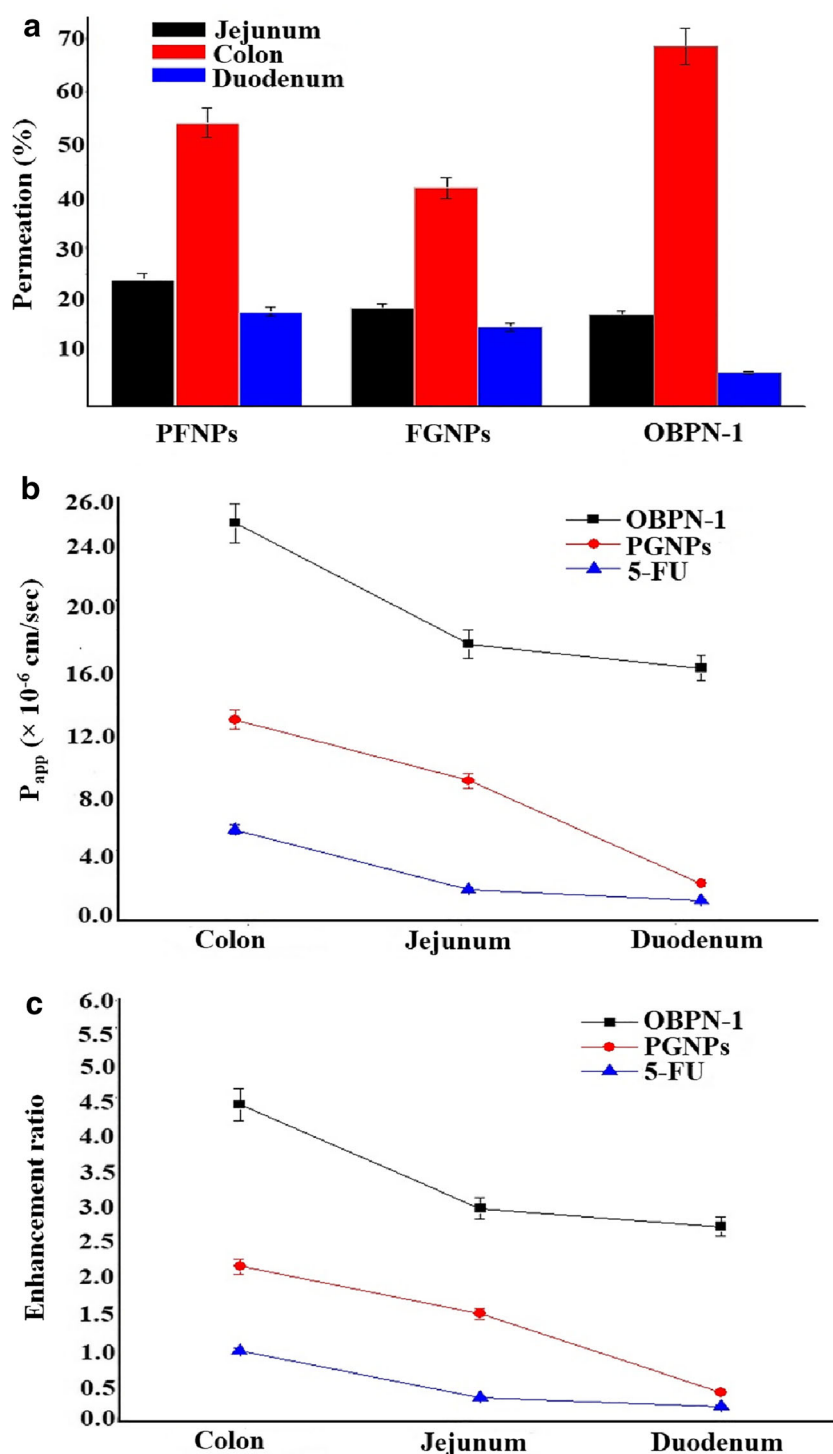
Fig. 11. *Ex vivo* permeation of 5-FU across the rat duodenum, jejunum and colon from the respective formulations: **a** permeation profile (%) of the formulations, **b** apparent permeability coefficient, and **c** enhancement ratio as compared with drug solution

colon. The pluronic-coated OBPN-1 demonstrated 4.6-fold higher permeation across the jejunum over 24 min compared with the DS (Fig. 11a), possibly due to the impregnated hydrophilic 5-FU inside the pluronic coating over the gold core. The hydrophilic nature of the drug hinders its permeation across the lipophilic mucosal membrane after mixing with the hydrophilic mucosal content. Therefore, the mucosal

tissue is an ideal site for absorption of hydrophobic drugs, whereas the hydrophilic mucosal environment favors emulsification of hydrophilic drug molecules. This may be a reason for the ~80% degradation of 5-FU observed at the absorption site, which presents a great challenge for the formulation of effective 5-FU-loaded nanomedicines (61). Thus, formulation scientists are still striving to tailor 5-FU-loaded novel carriers

for successful delivery to the systemic circulation with an improved pharmacokinetic profile having low toxicity or that is free from the dose-dependent complications occurring with the conventional dosage forms.

5-FU presents various values of apparent permeability coefficients (P_{app}) across the intestinal, which are species-dependent. The value of the P_{app} of 5-FU across human Caco-2 monolayer cells was 5.5×10^{-6} cm/s at 1.1×10^{-4} M concentration (62). Theoretically, the coefficient varies according to the physicochemical properties of the drug such as particle size, lipophilicity, functionalization, and molecular weight. The molecular weight of 5-FU is 130.6 g/mol suggesting a low and small hydrophilic molecule which is absorbed primarily through the tight junction of the intestinal mucosal membrane. The results of the apparent permeability coefficient of the 5-FU solution, FGNPs and optimized OBPN-1 were 1.3×10^{-6}, 2.4×10^{-6} and 16.1×10^{-6} cm/s in rat colon, respectively (Fig. 11b). The "P_{app}" values of the OBPN-1 were 25.3×10^{-6}, 17.6×10^{-6} and 16.1×10^{-6} cm/s for the colon, jejunum, and duodenum, respectively. These values indicated that there was progressive decrease in the permeability coefficient from the proximal portion to the distal portion of the gastrointestinal tract, which may be due to pH, variation in the intestinal anatomical structure in the different segments (63). However, pluronic-coated OBPN-1 showed a significantly higher permeability coefficient for 5-FU across the duodenum, jejunum, and colon than pure DS (Fig. 11b). Similarly, enhancement ratios were also better for OBPN-1 than for the drug solution (Fig. 11c). These improvements may be correlated to the protective effect of pluronic capped over drug-loaded gold NPs and the increase in permeability in the order colon jejunum duodenum (63).

Recently, few authors explored biosurfactant (sucrose laurate) and FDA (Food and Drug Administration) approved surfactant (labrasol) for improved intestinal permeation across rat intestine (64, 65). Labrasol (non-ionic surfactant) enhanced the transport of the paracellular marker (mannitol) across the rat colonic mucosae and permeation was non-damaging, transient and depended upon molecular weight (65). Similarly, sucrose laurate enhanced permeation of mannitol across the colonic tissue (64). In this study, we need to explore these biocompatible surfactants for increased intestinal permeation of 5-FU in higher rodents and large animal group. This future perspective may render informative data to scientists, scholar and academician working on related domain.

CONCLUSION

Based on the preliminary findings of PLGA-based NPs and pluronic-coated gold NPs for oral delivery of 5-FU, a robust formulation of gold NPs containing a precise amount of gold salt and CLS was required. These two prime components were significant factors influencing the physicochemical and physiological behavior of the drug-loaded gold NPs. Therefore, Design Expert software was applied (full factorial model) to identify optimum concentrations of both components to achieve a robust formulation under set constraints. The software predicted OBPN-1 as the optimum formulation having maximum desirability. OBPN-1 was evaluated for all responses and comparative investigations against PFNPs, and the PGNPs

exhibited significant efficacy against colon cancer cell lines. Biogenic pluronic-coated gold NPs were developed to overcome the adverse effects related to drug overdosing and the size restrictions of pure 5-FU microspheres for chemotherapy. These NPs were biosynthesized using *B. licheniformis* to improve polymer coating and loading efficiency. The nanoformulation exhibited biphasic drug release kinetics distinct from the pure DS, with delayed release to prolong time in the systemic circulation and enhance cellular uptake for cancer therapy. The GNPs improved the stability and biocompatibility of the nanoformulation and loaded drug, and increased cancer cell toxicity and *ex vivo* intestinal permeation compared with the PFNP nanoformulation. Thus, the OBPN-1 nanoformulation represents a promising strategy for oral delivery of chemotherapeutics to treat colon cancer.

COMPLIANCE WITH ETHICAL STANDARDS

Conflict of Interest The authors declare that they have no conflict of interest.

REFERENCES

1. World Health Organization (WHO) (2018) https://www.who.int/news-room/fact-sheets/detail/cancer).
2. Torre LA, Siegel RL, Jemal AL. Lung cancer statistics: in lung cancer and personalized medicine. Springer Cham. 2016;893:1–9.
3. Daga A, Ansari A, Patel S, Mirza S, Rawal R, Umrania V. Current drugs and drug targets in non-small cell lung cancer: limitations and opportunities. Asian Pac J Cancer Prev. 2015;16(10):4147–56.
4. Guo T, Holzberg TR, Lim CG, Gao F, Gargava A, Trachtenberg JE, et al. 3D printing PLGA: a quantitative examination of the effects of polymer composition and printing parameters on print resolution. Biofabrication. 2017;9(2):12–23.
5. Huang CY, Ju DT, Chang CF, Reddy PM, Velmurugan BK. A review on the effects of current chemotherapy drugs and natural agents in treating non–small cell lung cancer. Biomedicine. 2017;7(4):23. https://doi.org/10.1051/bmdcn/2017070423.
6. Lee JJ, Beumer JH, Chu E. Therapeutic drug monitoring of 5-fluorouracil. Cancer Chemother Pharmacol. 2016;78(3):447–64.
7. Chaudhary S, Umar A, Mehta SK. Surface functionalized selenium nanoparticles for biomedical applications. J Biomed Nanotechnol. 2014;10(10):3004–42.
8. Liu W, Li X, Wong YS, Zheng W, Zhang Y, Cao W, et al. Selenium nanoparticles as a carrier of 5-fluorouracil to achieve anticancer synergism. ACS Nano. 2012;6(8):6578–91.
9. Ohya Y, Takei T, Kobayashi H, Ouchi T. Release behaviour of 5-fluorouracil from chitosan-gel microspheres immobilizing 5-fluorouracil derivative coated with polysaccharides and their cell specific recognition. J Microencapsul. 1993;10(1):1–9.
10. Wen H, Jung H, Li X. Drug delivery approaches in addressing clinical pharmacology-related issues: opportunities and challenges. AAPS J. 2015;17(6):1327–40.

11. Gentile P, Chiono V, Carmagnola I, Hatton P. An overview of poly (lactic-co-glycolic) acid (PLGA)-based biomaterials for bone tissue engineering. Int J Mol Sci. 2014;15(3):3640–59.

12. Safwat MA, Soliman GM, Sayed D, Attia MA. Gold nanoparticles enhance 5-fluorouracil anticancer efficacy against colorectal cancer cells. Int J Pharm. 2016;513(1–2):648–58.

13. Alakhov V, Kabanov A. Block copolymer-based formulations of doxorubicin efective against drug resistant tumours, in Biomedical Polymers and Polymer Therapeutics, E. Chiellini, J. Sunamoto, C. Migliaresi, R. M. Ottenbrite, and D. Cohn, Eds., pp. 121–137, Kluwer Academic, New York, NY, USA, 2002.

14. Kabanov AV, Batrakova EV, Alakhov VY. Pluronic block copolymers as novel polymer therapeutics for drug and gene delivery. J Control Release. 2002;82(2–3):189–212.

15. Alakhov VY, Moskaleva EY, Batrakova EV, Kabanov AV. Hypersensitization of multidrug resistant human ovarian carcinoma cells by pluronic P85 block copolymer. Bioconjug Chem. 1996;7(2):209–16.

16. Han J, Zhao D, Li D, Wang X, Jin Z, Zhao K. Polymer-based nanomaterials and applications for vaccines and drugs. Polymers. 2018;10(1):1–14.

17. Martins C, Sousa F, Araujo F, Sarmento B. Functionalizing PLGA and PLGA derivatives for drug delivery and tissue regeneration applications. Adv Healthc Mater. 2018;7(1):1701035. https://doi.org/10.1002/adhm.201701035.

18. Mu L, Feng SS. A novel controlled release formulation for the anticancer drug paclitaxel (Taxol®): PLGA nanoparticles containing vitamin E TPGS. J Control Release. 2003;86(1):33–48.

19. Lee SY, Cho HJ. Dopamine-conjugated poly (lactic-co-glycolic acid) nanoparticles for protein delivery to macrophages. J Colloid Interface Sci. 2017;490:391–400.

20. Cleland JL, Mac A, Boyd B, Yang J, Duenas ET, Yeung D, et al. The stability of recombinant human growth hormone in poly (lactic-co-glycolic acid) (PLGA) microspheres. Pharm Res. 1997;14(4):420–5.

21. Dai J, Long W, Liang Z, Wen L, Yang F, Chen G. A novel vehicle for local protein delivery to the inner ear: injectable and biodegradable thermosensitive hydrogel loaded with PLGA nanoparticles. Drug Dev Ind Pharm. 2018;44(1):89–98.

22. Bailey BA, Desai KG, Ochyl LJ, Ciotti SM, Moon JJ, Schwendeman SP. Self-encapsulating poly (lactic-co-glycolic acid) (PLGA) microspheres for intranasal vaccine delivery. Mol Pharm. 2017;14(9):3228–37.

23. Silva AL, Soema PC, Slütter B, Ossendorp F, Jiskoot W. PLGA particulate delivery systems for subunit vaccines: linking particle properties to immunogenicity. Hum Vaccines Immunother. 2016;2(4):1056–69.

24. Boisselier E, Astruc D. Gold nanoparticles in nanomedicine: preparations, imaging, diagnostics, therapies and toxicity. Chem Soc Rev. 2009;38:1759–82.

25. Safwat MA, Soliman GM, Sayed D, Attia MA. Gold nanoparticles capped with benzalkonium chloride and poly (ethylene imine) for enhanced loading and skin permeability of 5-fluorouracil. Drug Dev Ind Pharm. 2017;43(11):1780–91.

26. Safwat MA, Soliman GM, Sayed D, Attia MA. Fluorouracil-loaded gold nanoparticles for the treatment of skin cancer: development, in vitro characterization, and in vivo evaluation in a mouse skin cancer xenograft model. Mol Pharm. 2018;15(6):2194–205.

27. Mohammad O, Faisal SM, Ahmad N, Rauf MA, Umar MS, Mujeeb AA, Pachauri P, Ahmed A, Kashif M, Ajmal M, Zubair S. Bio-mediated synthesis of 5-FU based nanoparticles employing orange fruit juice: a novel drug delivery system to treat skin fibrosarcoma in model animals. Sci Rep. 2019; 23;9(1):12288.

28. Singh S, Vidyarthi AS, Nigam VK, Dev A. Extracellular facile biosynthesis, characterization and stability of gold nanoparticles by *Bacillus licheniformis*. Artif Cells Nanomed Biotechnol. 2014:1–7.

29. Sharma N, Pinnaka AK, Raje M, FNU A, Bhattacharyya MS, Choudhury AR. Exploitation of marine bacteria for production of gold nanoparticles. Microb Cell Factories. 2012;11:86.

30. Murawala P, Tirmale A, Shiras A, Prasad BLV. In situ synthesized BSA capped gold nanoparticles: effective carrier of anticancer drug methotrexate to MCF-7 breast cancer cells. Mater Sci Eng C. 2014;34:158–67.

31. Zhang Z, Wang X, Li B, Hou Y, Yang J, Yi L. Development of a novel morphological paclitaxel-loaded PLGA microspheres for effective cancer therapy: in vitro and in vivo evaluations. Drug Deliv. 2018;25(1):166–77.

32. Ahmad N, Alam MA, Ahmad R, Naqvi AA, Ahmad FJ. Preparation and characterization of surface-modified PLGA-polymeric nanoparticles used to target treatment of intestinal cancer. Artif Cells Nanomed Biotechnol. 2018;46(2):432–46.

33. Pan X, Zhang X, Sun H, Zhang J, Yan M, Zhang H. Autophagy inhibition promotes 5-fluorouraci-induced apoptosis by stimulating ROS formation in human non-small cell lung cancer A549 cells. PLoS One. 2013;8(2):e56679.

34. Hussain A, Haque MW, Singh SK, Ahmed FJ. Optimized permeation enhancer for topical delivery of 5-fluorouracil-loaded elastic liposome using design expert: part II. Drug Deliv. 2015;23(4):1242–53.

35. Dash V, Mishra SK, Singh M, Goyal AK, Rath G. Release kinetic studies of aspirin microcapsules from ethyl cellulose, cellulose acetate phthalate and their mixtures by emulsion solvent evaporation method. Sci Pharm. 2010;78(1):93–102.

36. Hussain A, Altamimi MA, Alshehri S, Imam SA, Shakeel F, Singh SK. Novel approach for transdermal delivery of rifampicin to induce synergistic anti-mycobacterial effects against cutaneous and systemic tuberculosis using a cationic nanoemulsion gel. Int J Nanomedicine. 2020;15:1073–94.

37. Hussain A, Singh SK, Singh N, Verma PRP. In vitro-in vivo in-silico simulation studies of anti-tubercular drugs doped with self-nanoemulsifying drug delivery system. RSC Adv. 2016;6:93147–61.

38. Ruan LP, Chen S, Yu BY, Zhu DN, Cordell GA, Qiu SX. Prediction of human absorption of natural compounds by the non-everted rat intestinal sac model. Eur J Med Chem. 2006;41(5):605–10.

39. Kumari M, Mishra A, Pandey S, Singh SP, Chaudhry V, Mudiam MKR, et al. Physicochemical condition optimization during biosynthesis lead to development of improved and catalytically efficient gold nano particles. Sci Rep. 2016;6:1–14.

40. Newton DW, Kluza RB. pKa values of medicinal compounds in pharmacy practice. Ann Pharmacother. 1978;12:546–54.

41. Arias J. Novel strategies to improve the anticancer action of 5-fluorouracil by using drug delivery systems. Molecules. 2008;13:2340–69.

42. Ortiz R, Prados J, Melguizo C, Arias JL, Ruiz MA, Álvarez PJ, et al. 5-fluorouracil-loaded poly(ε-caprolactone) nanoparticles combined with phage E gene therapy as a new strategy against colon cancer. Int J Nanomedicine. 2012;7:95–107.

43. Gerweck LE, Vijayappa S, Kozin S. Tumor pH controls the in vivo efficacy of weak acid and base chemotherapeutics. Mol Cancer Ther. 2006;5:1275–9.

44. Sun SB, Liu P, Shao FM, Miao QL. Formulation and evaluation of PLGA nanoparticles loaded capecitabine for prostate cancer. Int J Clin Exp Med. 2015;8(10):19670–81.

45. Matai I, Sachdev A, Gopinath P. Multicomponent 5-fluorouracil loaded PAMAM stabilized-silver nanocomposites synergistically induce apoptosis in human cancer cells. Biomater Sci. 2015;3(4):457–68.

46. Kim D, Jeong YY, Jon S. A drug-loaded aptamer - gold nanoparticle bioconjugate for combined CT imaging and therapy of prostate cancer. ACS Nano. 2010;4:3689–96.

47. Kulkarni SA, Feng SS. Effects of particle size and surface modification on cellular uptake and biodistribution of polymeric nanoparticles for drug delivery. Pharm Res. 2013;30(10):2512–22.

48. Jain N, Bhargava A, Panwar J. Enhanced photocatalytic degradation of methylene blue using biologically synthesized "proteincapped" ZnO nanoparticles. Chem Eng. 2014; J 243: 549–555.

49. Giteau A, Venier-Julienne MC, Aubert-Pouëssel A, Benoit JP How to achieve sustained and complete protein release from PLGA-based microparticles Int J Pharm 2008; 350: 14–26.

50. Udofot O, Affram K, Bridg'ette Israel EA. Cytotoxicity of 5-fluorouracil-loaded pH-sensitive liposomal nanoparticles in colorectal cancer cell lines. Integr Cancer Sci Ther. 2015;2:245.

51. Sylvestre JP, Kabashin AV, Sacher E, Meunier M, Luong JH. Nanoparticle size reduction during laser ablation in aqueous solutions of cyclodextrins, lasers and applications in science and engineering. Int Soc Opt Eng. 2004:84–92.

52. Bonengel S, Bernkop-Schnürch A. Thiomers—from bench to market. J Control Release. 2014;195:120–9.

53. Bhattacharjee S. DLS and zeta potential—what they are and what they are not? J Control Release. 2016;235:337–51.

54. Jeong B. Injectable biodegradable materials. In:Injectable biodegradable materials. Injectable Biomaterials: Woodhead Publishing Limited; 2011. p. 323–237. https://doi.org/10.1533/9780857091376.3.323.

55. Salama AH, Mahmoud AA, Kamel R. A novel method for preparing surface-modified Fluocinolone Acetonide loaded PLGA nanoparticles for ocular use: in vitro and in vivo evaluations. AAPS PharmSciTech. 2015;17(5):1159–72.

56. Leelakanok N, Geary S, Salem A. Fabrication and use of PLGA-based formulations designed for modified release of 5-fluorouracil. J Pharm Sci. 2018;107(2):513–28.

57. Alruwaili NK, Zafar A, Imam SS, Alharbi KS, Alshehri S, Elsamam T, Alomar FA, Akhtar S, Fahmi UA, Alhakamy NAA, Alshammari MS. Formulation of amorphous ternary solid dispersion of dapagliflozin using PEG 6000 and poloxamer 188: Solid-state characterization, ex vivo study, and molecular simulation assessment. Drug Development and Industrial Pharmacy. 2020: early online, doi: https://doi.org/10.1080/03639045.2020.1802482.

58. Singh R, Kesharwani P, Mehra NK, Singh S, Banerjee S, Jain NK. Development and characterization of folate anchored Saquinavir entrapped PLGA nanoparticles for anti-tumor activity. Drug Dev Ind Pharm. 2015;41(11):1888–901.

59. Hirsch LR, Stafford RJ, Bankson JA, Sershen SR, Rivera B, Price RE, et al. Nanoshell-mediated near-infrared thermal therapy of tumors under magnetic resonance guidance. PNAS. 2003;100:13549–54.

60. Kuroda K, Caputo GA. Antimicrobial polymers as synthetic mimics of host-defense peptides. WIREs Nanomed Nanobiotechnol. 2012;5:49–66.

61. Omura K. Clinical implications of dihydropyrimidine dehydrogenase (DPD) activity in 5-FU-based chemotherapy: mutations in the DPD gene, and DPD inhibitory fluoropyrimidines. Int J Clin Oncol. 2003;8:132–8.

62. Buur A, Trier L, Magnusson C, Artursson P. Permeability of 5-fluorouracil and prodrugs in caco-2 cell monolayers. Int J Pharm. 1996;29:223–31.

63. Artursson P, Ungell AL, Lofroth E. Selective paracellular permeability in two models of intestinal absorption: cultured monolayers of human intestinal epithelial cells and rat intestinal segments. Pharm Res. 1993;10:1123–9.

64. McCartney F, Rosa M, Brayden DJ. Evaluation of sucrose Laurate as an intestinal permeation enhancer for macromolecules: ex vivo and in vivo studies. Pharmaceutics. 2019;11:565. https://doi.org/10.3390/pharmaceutics11110565.

65. McCartney F, Janninb V, Chevrier S, Boulghobra H, Hristova DR, Ritter N, et al. Labrasol® is an efficacious intestinal permeation enhancer across rat intestine: ex vivo and in vivo rat studies. J Control Release. 2019;310:115–26.